Journal of Magnetic Resonance **136,** 102–113 (1999)
Article ID jmre.1998.1629, available online at http://www.idealibrary.com on IDEAL®

Using Flow Relaxography to Elucidate Flow Relaxivity

Jing-Huei Lee,*,[1] Xin Li,† Manoj K. Sammi,† and Charles S. Springer, Jr.*,†

*Chemistry Department, Brookhaven National Laboratory, Upton, New York 11973; and †Department of Chemistry, State University of New York, Stony Brook, New York 11794

Received September 25, 1998

We have investigated the theoretical and experimental linear dependence of the reciprocal of the apparent longitudinal relaxation time [$(T_1^*)^{-1}$] of the NMR signal from spins in a flowing fluid on the volume flow rate, F_v, the so-called *inflow effect*. We refer to the coefficient of this dependence as the longitudinal *flow relaxivity*, r_{1F}. A very simple model predicts that, under a range of conditions pertinent to modern flow studies and perfusion imaging experiments, r_{1F} is controlled by the volume of the fluid in which the magnetization is perturbed by pulsed RF inversion or saturation, not the detection volume, and that it can be approximated as the reciprocal of half of the inversion volume. Phantom sample experiments, using a new, quantitative approach that we call *flow relaxography*, confirm the general predictions of this simple model. There are two intriguing implications of these findings for general NMR flow studies as well as for medical applications. It should be possible to vary the value of r_{1F} by simply (noninvasively) adjusting the inversion slice thickness, and thus measure the value of (blood ^1H_2O, for example) F_v in a vessel without changing F_v, from the resultant varying T_1^* values. Also, it should be possible to extrapolate to the intrinsic T_1 value of the fluid signal (as if it were stationary), without altering or stopping the flow. Again, these are quite successful in phantom sample studies. Imaging versions of the flow relaxographic experiments are also possible. The twin goals of flow studies in medical MRI are the quantitative discrimination of the signals from flowing and nonflowing spins, and the accurate measurement of the flow rate of the former.

INTRODUCTION

It has been long known that flow can affect the apparent longitudinal relaxation time (T_1^*) of the magnetic resonance signal from spins in a fluid (*1–3*). The effect of flow (which involves coherent motion) will, in principle, not affect the intrinsic relaxation of NMR signals since the latter is due to random (incoherent) molecular motion. Consequently, flow will also not alter the intrinsic intensity of the NMR signal. However, the net magnetization of the sample in the region detected is altered if the molecules flowing into this region have a different magnetic or chemical nature than that of those flowing out (*2–4*). Fortunately, the determination of flow rate by NMR is possible without the injection of an exogenous tracer molecule (chemical tagging), because the *perturbed* flowing nuclear magnetization can be thought to act itself as an NMR tracer (endogenous tracer, or so-called magnetic "tagging"). The formation of the magnetic tagging can be consequent to nuclear magnetization or demagnetization by the static magnetic field ($\mathbf{B}_0$), or to magnetization saturation or inversion by the RF magnetic field ($\mathbf{B}_1$). It is on the basis of these NMR principles that flow effects include time-of-flight (*3, 5–9*), inflow/outflow (*1, 10–13*), phase modulation (*14–18*), or combinations of these (*19*). The basis of the time-of-flight method is to measure the time taken by tagged magnetization to travel the distance between two coils. This method provides flow velocity directly, but is difficult to implement *in vivo* (*9, 20*). The phase modulation method is relatively more complicated, has its own difficulties (e.g., phase aliasing and motion sensitivity (*21*)), and does not easily discriminate the contribution from water diffusion (*17, 22, 23*). To date, methods employing the inflow/outflow effect, with and without the time-of-flight effect, probably are the most commonly used. However, in order to quantify the flow rate precisely, one needs to know the intrinsic T_1 value of the signal from the flowing spins that would obtain if the fluid were stationary, along with the appropriate sensitive volume. Thus, most practical studies can provide only qualitative information.

In this report, we introduce the concept of the longitudinal flow relaxivity; and, along with using relaxographic approaches (*24, 25*), we are able to accurately measure the volume flow rate and the intrinsic T_1 value for the signal from a phantom sample.

THEORY

It has been known almost since the discovery of NMR that the coherent movement of a flowing fluid can alter the apparent longitudinal relaxation time of the signal arising from spins contained therein (*1, 10*). Under many conditions, this apparent relaxation time remains effectively single-valued; that is, the relaxation can be treated as monoexponential (*1, 2, 26*). As will be seen below we have confirmed this by applying a new,

[1] To whom correspondence should be addressed. Fax: (516) 344-5576. E-mail: jlee@bnl.gov.

1090-7807/99 $30.00

quantitative technique, *flow relaxography*, in an extensive set of inversion recovery experiments. Furthermore, the apparent relaxation rate constant is often linearly dependent on the volume flow rate, F_v (*2, 19, 26*). Although we are not aware that anyone has done so, this means that one can express this effect in a *relaxivity* equation

$$(T_1^*)^{-1} = (T_1)^{-1} + r_{1F} \cdot F_v, \qquad [1]$$

where T_1^* is the apparent relaxation time, T_1 is the intrinsic relaxation time (as if the fluid were stationary), and r_{1F} can be termed the *longitudinal flow relaxivity.*

From dimensional analysis, it is clear that r_{1F} must have the dimension of reciprocal volume $[(V^*)^{-1}]$: F_v has dimensions of (volume/time). Thus, the product $r_{1F} \cdot F_v$ is a reciprocal time constant $[(t_F)^{-1}]$. The prose characterizations of this time constant in the literature have varied. Thus, Denis *et al.* described it as (translated from the French) the "time necessary for a $1/e$ fraction of the saturated spins to flow out of the resonance volume" (*1*). Singer suggested that a derivation from a modified form of Bloch's differential equation leads to an interpretation of t_F as the mean time for a flowing spin in the detection volume (V_o) (*2*), which is not the same as that of the French group. Jones and Child repeated Singer's result (*26*), and Hemminga repeated Singer's stated derivation (*19*). The implication of the Singer interpretation is that $V^* = V_o$. As far as we are aware, these differing implications have never been carefully examined. Hemminga and coworkers did report a *transverse* relaxation study, in which they found the equivalent of r_{2F} to be $(1.4 \cdot V_o)^{-1}$ (*12*). They attributed this discrepancy (with *both* of the above interpretations) to an inhomogeneous $\mathbf{B}_1$ field, which had a particularly important effect on their transverse relaxation measurement. Perhaps a major reason that these ideas have not been tested is that, early on, it seemed difficult to do so. The value of V_o could ostensibly be varied only by employing a series of single-coil (or crossed-coil) transceiver systems of different dimensions. However, the introduction of the slice-selection concept by Garroway *et al.* (*27*) provided a facile way of accomplishing this test. We employ this approach in the present paper.

Before we present our results, however, let us revisit the theory with the simplest possible model. Figure 1a depicts a tube of cross-sectional area A, with fluid flowing from left to right. The detection volume will be determined by the slice thickness, S_o, selected for the read RF pulses applied during the recovery from inversion. The volume of fluid whose nuclear magnetization is inverted, V_i, can be independently controlled and varied by selecting the sample thickness, S_i, subjected to the inversion RF pulse. For the considerations here, these two slices will always have identical slab center planes (that of the RF coil). Assume that the magnetization inside V_i (which includes V_o) is inverted at time zero, and that the magnetization outside V_i is, and remains, at Boltzmann equilibrium (M_0, for $\mathbf{B}_0$ and T).

Figure 1b (left) illustrates the recovery of magnetization, after inversion, that is *due only to relaxation* (i.e., $F_v = 0$). It is a plot of the magnetization in V_o, $M_z(t)$, as a function of time after the inversion (i.e., $M_z(0) = -M_0$). The curve is that of a single exponential, with $T_1 = 1.13$ s in this case. In Fig. 1b (right), one sees the distribution of T_1 values that describes the recovery in 1b (left), the *longitudinal relaxogram* (*25*). As related under Experimental, this was obtained by submitting discrete points (coordinate pairs) from the recovery curve to the computer program CONTIN. This *relaxography* process is effectively the inverse Laplace transformation (ILT) of the recovery curve. Of course, the relaxogram returned by CONTIN is essentially a δ-function in this case.

In Fig. 1c (left) is shown the recovery of magnetization *due only to flow* (i.e., $T_1 = \infty$). The curves depict the ways that two different limiting flow velocity patterns change magnetization due to the flow of spins into and out of V_o. The solid and dotted lines represent the plug flow and Poisseuille (simple laminar) flow patterns, respectively. For the plug flow model, the magnetization starts at $-M_0$ after the inversion RF pulse, and remains as such until $t = 0.5\,(V_i - V_o)/F_v$, when M_0 fluid begins to enter V_o. Then it *linearly recovers* to M_0 as the plug with $-M_0$ is washed out of V_o. The time increment for all of the magnetization in V_o to reach M_0 is V_o/F_v. In this simulation, we chose $S_i = 2S_o$. For the laminar flow model, we used equivalent parameters (e.g., the average velocity in the laminar flow was set equal to that of the plug flow (*4, 19*)). The laminar flow model required following the increasing incursion of a volume of magnetization M_0 into V_o with an ever-growing front having the shape of a parabolic cone, and utilizing the volume-weighted distribution of flow velocities (*4, 19*). It is interesting to observe that, for both models, the magnetization reaches $1/e$ of the *difference* from equilibrium (M_0) of its *initial* value at the same time (the intersection of the two lines in Fig. 1c (left)). The abscissal value of this point is t_F, and the model parameters were chosen so that it equals 1.13 s (i.e., it is the same as T_1 in Fig. 1b (left)). The ILTs of the two curves in Fig. 1c (left) produce the relaxograms in Fig. 1c (right), presented with corresponding solid and dotted lines. These are essentially indistinguishable. Obviously, the main consequence of the shape difference in the curves in 1b (left) and 1c (left) is a broadening of the single relaxographic peaks in 1c (right) compared with that in 1b (right). The peak area is unchanged. This broadening is intuitive in the sense that one can think of the curves in 1c (left) as having contributions from components with both larger and smaller time constants than that of 1b (left). The fact that these components are not resolved in the resulting relaxograms, 1c (right), is a consequence of the "non-unique" nature of the ILT, and the necessarily numerical approximation to it (*25*). It is important to note, however,

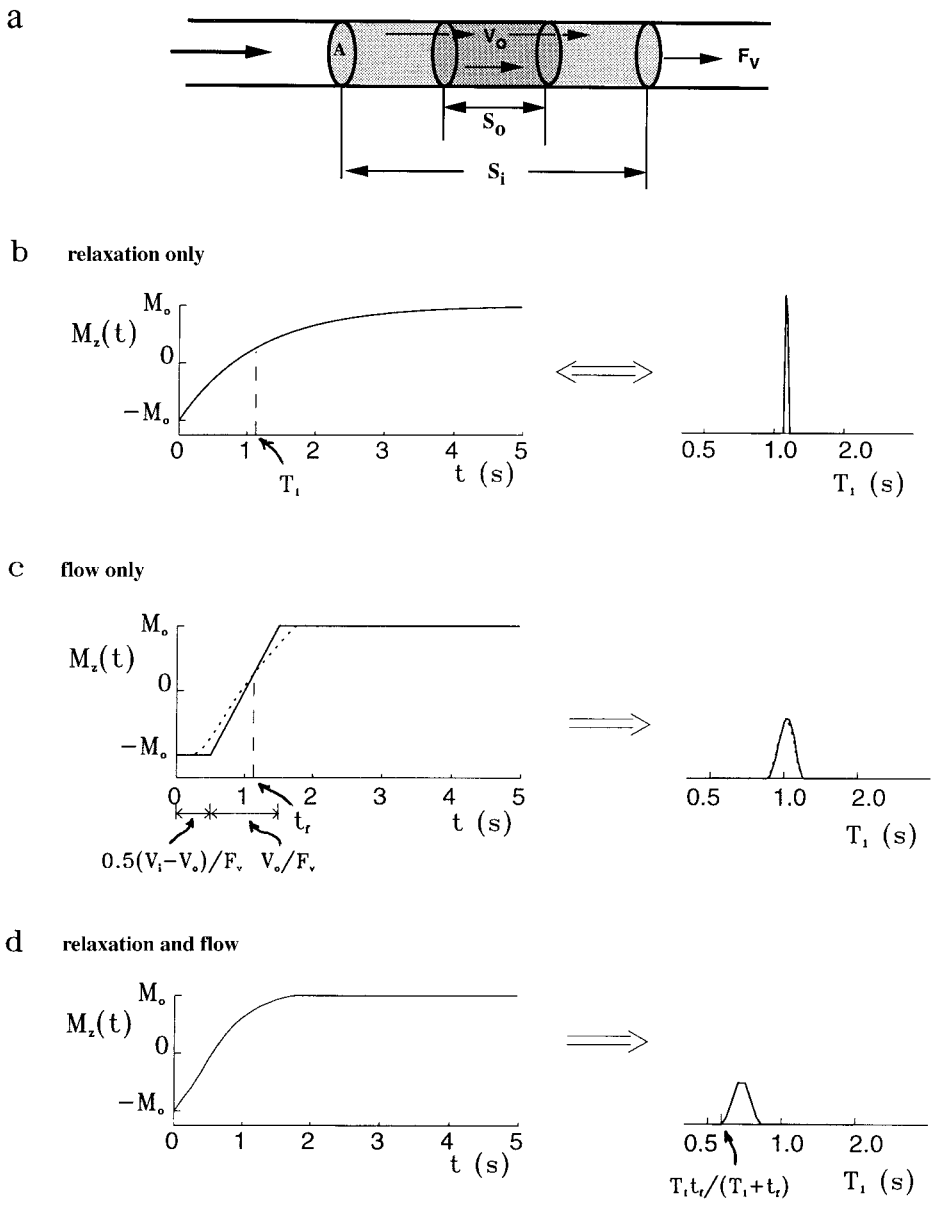

FIG. 1. (a) A drawing of a simple model for a fluid flowing in a cylindrical vessel. Some important parameters are indicated. (b) The time dependence of the recovery of longitudinal signal due to only relaxation with a single T_1 value of 1.13 s, and the relaxogram that is its inverse Laplace transform. (c) The recovery associated with only flow. The solid and dotted lines represent the recoveries caused by plug flow and simple laminar flow, respectively. These yield essentially identical longitudinal relaxograms. (d) The recovery due to simultaneous relaxation and plug flow, and its relaxogram.

that the two flow patterns represented in Fig. 1c actually bracket the cases of turbulent flow (*19*), and thus are the *limits* of practical flow patterns for most reasonable situations. There are imaging pulse sequences that can discriminate velocity patterns in the flow of a fluid though a large vessel (*18*). The transform arrow in Fig. 1c is not double-headed because the LT of the relaxogram of 1c (right) is a smoother curve more like the laminar flow recovery in 1c (left) than the plug flow recovery, but not exactly identical to either of them.

In Fig. 1d (left), we have convolved the relaxation and plug flow recoveries of 1b and 1c. The ILT of this curve, in Fig. 1d (right), shows a single broadened relaxographic peak that has been shifted to a position approaching the value $T_1t_F(T_1 + t_F)^{-1}$ (note the log scale for the abscissa). Let us derive this latter quantity.

In the wide range of conditions under which the measured recovery is empirically single exponential, we may use a simple exponential theory. Thus, we can model the change of magnetization due to the recovery from inversion, and the change of magnetization due to the flow into and flow out of V_o as *parallel* pseudo-first-order kinetic processes (the two

terms on the RHS of Eq. [1]). These are shown, respectively as

$$M_z(0) \xrightarrow{T_1^{-1}} M_0 \quad [2]$$

$$M_z(0) \xrightarrow{t_F^{-1}} M_0. \quad [3]$$

The expanded differential form of the Bloch rate law can thus be written as

$$\frac{dM_z(t)}{dt} = \frac{M_0 - M_z(t)}{T_1} + \frac{M_0 - M_z(t)}{t_F}, \quad [4]$$

and, from our definition of T_1^* given above, simplified as

$$\frac{dM_z(t)}{dt} = \frac{M_0 - M_z(t)}{T_1^*}. \quad [5]$$

A definite integration of Eq. [5] leads to

$$\frac{M_z(t) - M_o}{M_z(0) - M_o} = \exp\left(-\frac{t}{T_1^*}\right) = \exp\left(-\frac{t}{T_1}\right) \cdot \exp\left(-\frac{t}{t_F}\right). \quad [6]$$

Of course, T_1^* is given by $(T_1^{-1} + t_F^{-1})^{-1}$, which is the $T_1 t_F (T_1 + t_F)^{-1}$ position marked on the abscissa of Fig. 1d (right).

Thus, t_F is properly described as the time required for the difference from its equilibrium magnitude of the instantaneous magnetization inside V_o $[M_z(t)]$ to decrease to $1/e$ of its initial value, *because of flow*. Since t_F is V^*/F_v (from above), we can now write the correct expression for V^*, for the configuration of Fig. 1a, as

$$V^* = [1 - (1/e)]V_o + [(V_i/2) - (V_o/2)]. \quad [7]$$

This can be easily understood in terms of the plug flow model because t_F is the time required for the upstream (trailing) edge of the V_i plug to reach the point $1 - (1/e)$, 0.63, of the way through V_o. Another way to visualize this is to use a *flowing frame* of reference, in which the fluid is stationary and V_o moves to the left (in Fig. 1a) at F_v. In this picture, t_F is the time required for the upstream edge of V_o to move past the upstream edge of V_i, and further, to a point where 0.63 of V_o is out of V_i. Equation [7] simplifies to

$$V^* = 0.50\ V_i + 0.13\ V_o. \quad [8]$$

We see that, perhaps surprisingly, the V_o contribution to V^* is largely canceled. In fact, when V_i is noticeably larger than V_o, a simple approximation allows us to drop the V_o contribution to the flow relaxivity altogether. We will show that our experimental results are consistent with these predictions. On the other hand, when $V_i = V_o$, which was the case for most early experiments, Eq. [8] reduces to $V^* = 0.63\ V_o$. Note that this is not the same as either the French (*1*) [$V^* = 0.37\ V_o$] or the Singer (*2*) [$V^* = V_o$] interpretations. However, as pointed out above, these interpretations were never really tested.

EXPERIMENTAL

Two cylindrical tubes filled with saline solutions (150 mM NaCl) were placed inside a 4.7-cm long circularly polarized birdcage RF coil (ID = 4 cm) and oriented parallel to $\mathbf{B}_0$. One tube was made of glass (ID = 4.85 mm) and was sealed at both ends. The other tube (ID = 3.76 mm) was made of polyethylene, and one end was connected to an infusion pump (Harvard Apparatus, South Natick, MA) while the other end was drained into a large glass container. A drawing of the flow phantom is shown in Fig. 2a. The infusion pump was kept outside of the Faraday (RF) shielded room, and the polyethylene tubing was fed from it through an RF quarter-wave filter and formed into a spin polarizing coil about 10 ft in length near the center of the magnet bore before it entered the RF coil. The infusion pump was calibrated before the studies. The error of the flow setting for the full range was within 5% (data not shown).

All studies were performed with a 4-T Varian/Siemens whole-body instrument, and utilized a 10-cm (ID) home-made gradient insert. The T_1^* value was measured by using the PURR (*p*rogressively *u*nsaturated *r*elaxation during perturbed *r*ecovery from inversion) pulse sequence (*25*) with only one dimension of spatial encoding (a transverse (Y) projection of the two tubes). Following an inversion pulse (with or without Z slice selection), 64 Z slice-selective 5° read (observe) pulses were applied and (echo) data were collected immediately after each pulse (Fig. 2 of Ref. (*25*)). The 5° read pulse flip angle was sufficiently small to avoid affecting the T_1^* value by Look–Locker perturbation (*25*). Sinc-shaped pulses of duration 1.024 ms were used for the read and inversion irradiations, respectively, with their amplitudes appropriately adjusted. Consequently, the band widths of the read and inversion excitations were 5.8 and 4.3 kHz, respectively. The slice-selective Z gradient strengths for the read and inversion pulses were adjusted accordingly, and the slice thickness values were determined. Constant-flow experiments were conducted in two groups. In Group I, the read slice thickness (S_o) was kept at 10 mm, while the inversion slice thickness (S_i) was varied. In Group II studies, S_o was varied, while S_i was kept constant. In both groups, the read and inversion slab center planes were the same as that of the RF coil. The transverse field of view (FOV) was 20 mm, the repetition time (TR) 12 ms, the echo time (TE) 5.5 ms, and the inversion recovery time (TI) varied from 38 ms to 21 s with spacing increasing logarithmically (*25*).

All raw (echo) data were first Fourier transformed, and the

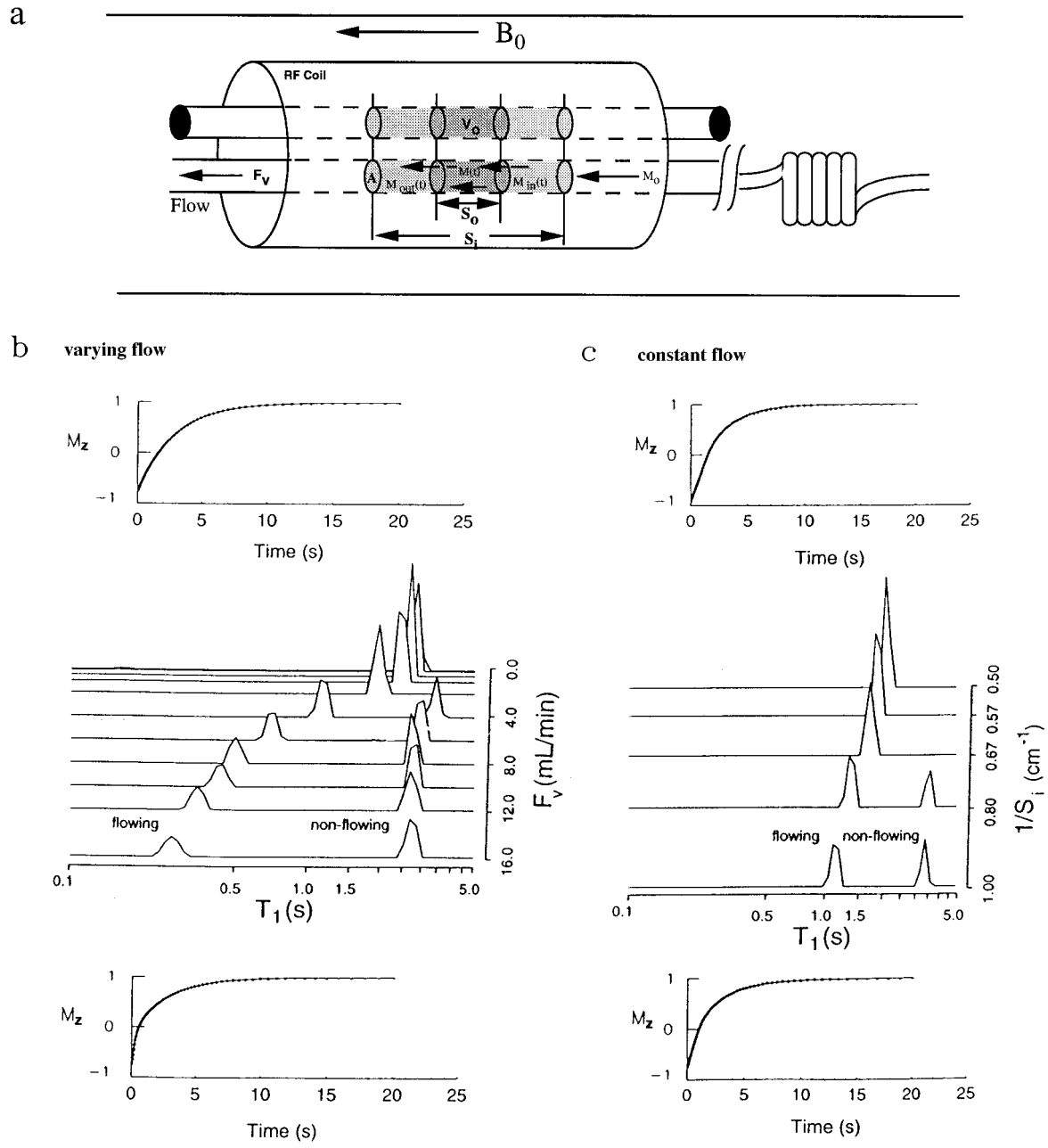

FIG. 2. (a) A drawing of the flow phantom in which there were two saline-filled tubes placed inside an RF coil. One tube was sealed at both ends, while the other has fluid running through it with a volume flow rate of F_v, after passing through a large spin polarizing coil (see text for details). (b) Flow ^1H_2O longitudinal relaxograms obtained from the two-tube phantom with increasing F_v. The stacked plot represents data obtained with a slice-selective inversion such that $S_o = S_i$ (=12.5 mm). The ordinate shows the volume flow rate in mL/min. At the top and the bottom are shown the inversion recovery data (filled circles) for the experiments with $F_v = 0.0$ and 16 mL/min, respectively. The solid lines through the data are the effective Laplace transforms of the corresponding relaxograms in the stacked plot. (c) Flow longitudinal relaxograms obtained with constant F_v (4.0 mL/min) and different S_i values. The stacked plot in the center has $1/S_i$ as the ordinate axis. At the top and the bottom are shown the inversion recovery data (filled circles) for the studies with $1/S_i = 0.5$ and 1.0 cm^{-1}, respectively. The solid lines through the data are the effective Laplace transforms of the topmost and bottommost relaxograms in the stacked plot.

resulting complex (projection) data were phased by using Interactive Data Language (IDL; Research Systems, Inc., Boulder, CO) software. Then, projection from three different regions of interest (ROI), one spanning both tubes and one for each tube individually, were integrated before the integral decay data were analyzed by CONTIN. The latter provides a statistical nonparametric approach that is "not predicated on specific model assumptions" (*25*). For example, this numerical "grid-method" produces distributions of relaxation times without positing discrete exponential components. There is at least

one other similar program available (*28*). The abscissae of the longitudinal relaxograms in this paper measure log T_1 (really, log T_1^*), and the ordinates are corrected to present "equal area" displays, in which peak areas may be planimetrically compared (*25*).

RESULTS

Figure 2b shows a stacked plot of the longitudinal relaxograms obtained from experiments in which the volume flow rate, F_v, in the polyethylene tube was varied from 0.0 to 16 mL/min, while the inversion slice selection width was kept constant at 12.5 mm (i.e., $1/S_i = 0.80\ cm^{-1}$), the same as the observe selection width, S_o. The abscissa is linear in the log of the T_1^* value, and the global vertical axis of the stacked plot measures F_v. These represent relaxographic results obtained by analyzing data from the ROI spanning both tubes. When the water in the polyethylene tube is stationary ($F_v = 0.0$ mL/min, top), only a single relaxographic peak is observed. Above the stacked plot are shown the inversion recovery data points (filled circles) from the experiment with $F_v = 0.0$ mL/min. The solid line (essentially indistinguishable from the points) is the effective LT of the top relaxogram. The root mean square value (b) of the residuals, relative to the full ordinate range of 2, is 0.62%. As the value of F_v increases, the initial single peak shifts to lower T_1^* values, and two peaks have emerged when the F_v value has reached 4.0 mL/min. The peak at the smaller apparent T_1 value (T_{1S}) in the relaxogram can be clearly assigned to the signal of the flowing water and that at the large T_1 value (T_{1L}) to nonflowing water. This is confirmed below. The data points (filled circles) from the $F_v = 16$ mL/min experiment are shown at the bottom, and the value of b for the solid line there is 1.43%. It is interesting to see a single relaxographic peak from the NMR signal of a flowing sample: the individual spins in the ensemble giving rise to the signal are continually changing. The graphic nature of flow relaxography is quite unique and important.

Figure 3a depicts plots of the relaxographic results of Fig. 2b ($S_o = S_i$), the results of experiments analogous to those of Fig. 2b but with a non-slice-selective inversion ($S_o < S_i$), and the results from the same experiments but with data taken from the ROI spanning only flowing water. The ordinate reports the value of the pseudo-first-order relaxation rate constant ($R_1^* = 1/T_1^*$) taken from the position of the relaxographic peak maximum. The filled and open symbols represent data from slice- and non-slice-selective inversion experiments, SS and NSS, respectively. The filled circles represent the position of the single peak of Fig. 2b (SS) before emergence and that of the T_{1S} peak after emergence while the open circles represent the analogous NSS case. The filled and open squares represent the position of the T_{1L} peak of Fig. 2b (SS) and the NSS case, respectively. The results from the case in which the relaxograms were obtained from the ROI with only flowing water are shown as filled and open diamonds for the SS and NSS studies, respectively. The dashed lines drawn in Fig. 3a are intended only to guide the eye. The good agreement between the diamonds and circles (both filled and open) demonstrates the reliableness and successfulness of the CONTIN analyses of the data from the ROI spanning both tubes (circles) and also serves to confirm the assignments of the relaxographic peaks therefrom. The inset shows the T_{1S} relaxographic peak area fraction values as filled and open triangles for results from experiments with SS (Fig. 2b) and NSS, respectively. The T_{1S} peak area fraction, $a_S/(a_S + a_L)$, decreases as F_v increases and reaches a plateau of about 0.40 when F_v is larger than 0.1 mL/s for the SS ($S_o = S_i$) case (Fig. 2b). This area fraction value of 0.40 is in excellent agreement with the actual fractional ID cross sectional area (A) of the polyethylene tube (relative to the sum of itself and that of the glass tube), which is 0.38. For the NSS case $S_o < S_i$), however, the F_v value must exceed 0.27 mL/s in order for $a_S/(a_S + a_L)$ to approach its plateau value. It is quite interesting to note that the peak area fraction curve shape is very different from that of a study of yeast cell suspensions using an extracellular relaxation regent (*25*). This difference is most likely due to the fact that the latter represents a case involving microscopic compartments in intimate contact, between which an equilibrium water exchange process is ongoing.

Figure 2c shows a stacked plot of longitudinal relaxograms obtained from a series of five Group I experiments during which the F_v value was kept *constant* at 4.0 mL/min (0.067 mL/s). In these experiments, the only experimental parameter varied was the thickness of the inversion slice, S_i. The global ordinate of the stacked plot is the reciprocal of this slice thickness, $1/S_i$ (in cm^{-1}). Thus, when $1/S_i$ is its smallest (topmost relaxogram), only one relaxographic peak is observed. Above the stacked plot are shown the inversion recovery data points (filled circles) from that experiment, with $1/S_i = 0.5\ cm^{-1}$. These represent relaxographic results obtained by analyzing data from a ROI containing both tubes. As before, the solid line is the effective LT of the topmost relaxogram and the b value of the residuals is 3.8%. As the value of $1/S_i$ is increased, the single relaxographic peak shifts to smaller T_1 values, and then splits into two peaks. Again, the T_{1S} peak represents the flowing spins while the T_{1L} peak is that of the signal from the nonflowing spins in the sealed tube. The data points (filled circles) from the $1/S_i = 1.0\ cm^{-1}$ experiment are shown below the bottom relaxogram. There, the value of b is only 1.6%. It is important to note that, in this experiment, the flow rate was unchanged. Thus, the T_1^* value of the flowing spin magnetization is changing because we are adjusting r_{1F} in Eq. [1], *not* F_v.

Figure 3b shows plots of R_1^* as functions of F_v (in mL/s) at different S_i values (the vertical arrays are Group I studies). The R_1^* values were obtained from the ROI containing only flowing water. The filled symbols represent data from experiments with S_i values of 10–30 mm, the slope decreasing with increasing S_i value. The solid lines drawn through them result from linear-

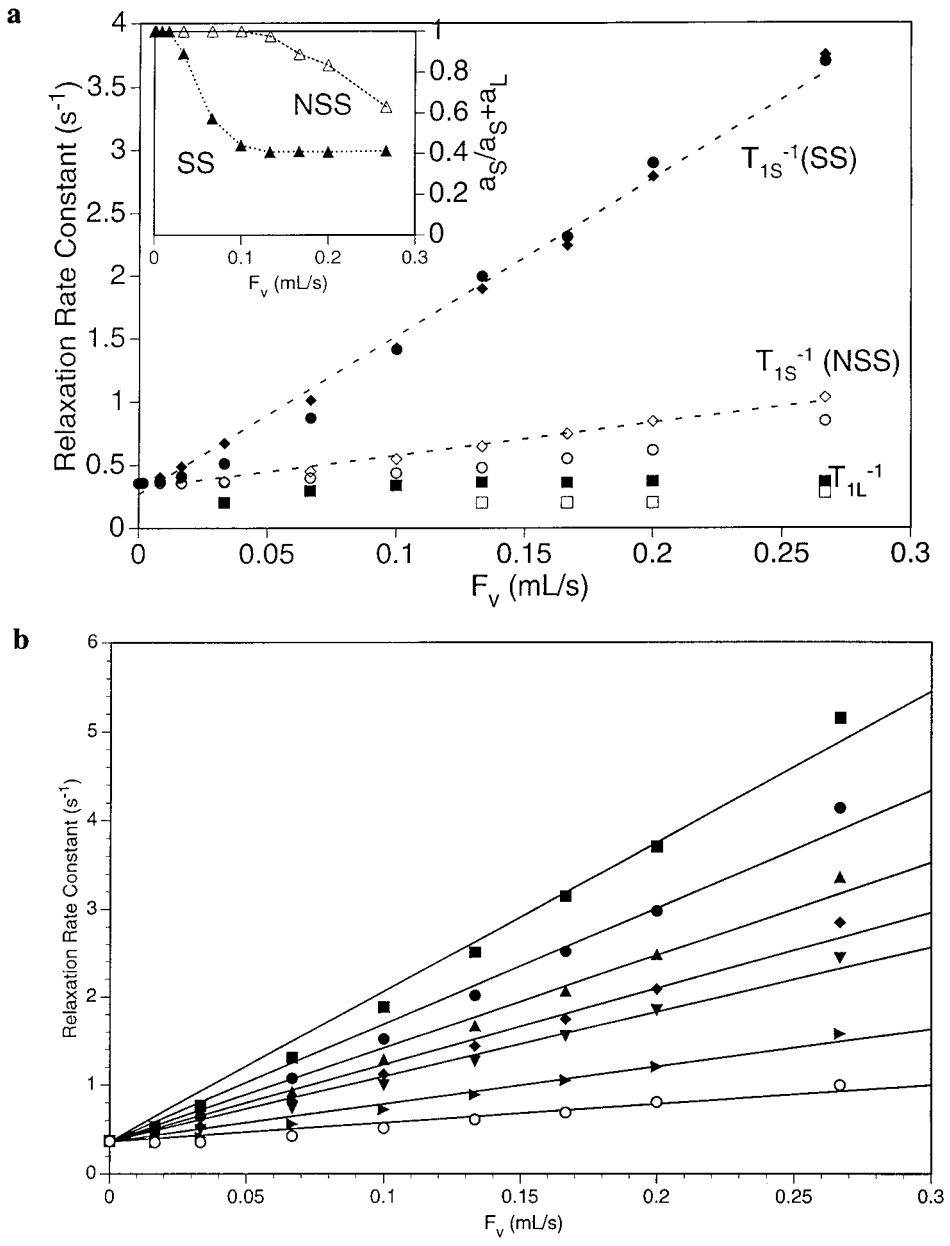

FIG. 3. (a) Plots of relaxographic peak parameters from slice-selective (SS) (Fig. 2b, $S_i = S_o$) and from analogous non-slice-selective (NSS) experiments ($S_i = 4S_o$, in the present case). Shown as well are the relaxographic results from the ROI spanning only the flowing water. The main graph shows the F_v dependence of the relaxographic peak positions (shown as reciprocal values on the ordinate, $R_1^* = 1/T_1^*$). The filled and open circles represent the single peak before emergence and the T_{1S} peak after emergence for the SS (Fig. 2b) and the NSS case, respectively. The filled and open squares represent the T_{1L} peak after emergence for the SS case (Fig. 2b) and NSS, respectively. The filled and open diamonds represent the values for the single peak from the ROI with only flowing water with the SS case and NSS case, respectively. The F_v dependence of the area fraction ($a_S/a_S + a_L$)) of the T_{1S} peak is shown in the inset (filled and open triangles for SS (Fig. 2b) and NSS, respectively). The dashed lines are intended only to guide the eye. (b) Plots of the first-order relaxation rate constant (R_1^*) as functions of F_v. The filled symbols represent data from experiments with S_i = 10.0, 12.5, 15.0, 17.5, 20.0, and 30.0 mm from top to bottom, respectively. The open circles represent data from an experiment with a non-slice-selective inversion. The solid lines drawn through them result from LLS fittings, and the slopes were the only variables.

least-squares (LLS) fittings. Only the slope was varied in each fitting. The intercept was kept at 0.363 s^{-1}, which is the reciprocal of the average T_1 value of all measurements of the nonflowing saline water signal ($n = 10$). The open circles represent data from experiments with the same parameters as those of the filled symbols except without a slice-selective gradient applied during the inversion pulse (i.e., $S_o < S_i$). The solid line drawn through them is the result of a LLS fitting with the same intercept fixed as above. The slope of this line is 2.42 mL^{-1}.

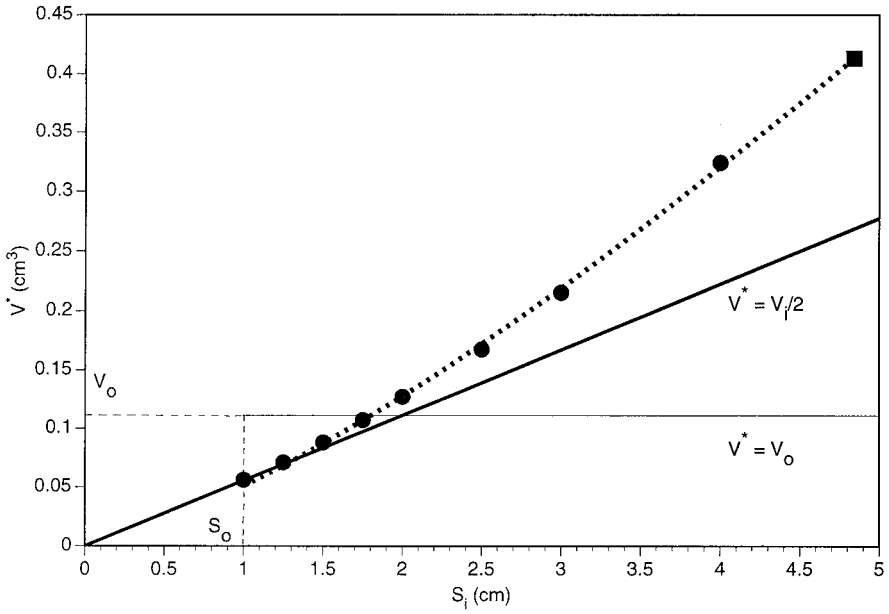

FIG. 4. Plots of the reciprocal of the slope values from Fig. 3b as a function of S_i. The ordinate is V^*. The bold solid line represents the values calculated from the first term on the RHS of Eq. [8]. The dotted line is the result of an LS fitting based on the empirical equation $V^* = \alpha S_i^{\beta}$ ($\alpha = 0.0508$; $\beta = 1.33$; r^2 is 0.999). A horizontal line for $V^* = V_o$ (implied in the literature) is also shown.

Figure 4 depicts a plot of V^*, the reciprocal of the slope values of the lines resulting from the slice-selective inversions in Fig. 3b, as a function of S_i (in cm). The dotted line is the result of a LS fitting for an empirical equation $V^* = \alpha \cdot S_i^{\beta}$. The coefficient α is 0.0508, β is 1.33, and $r^2 = 0.999$. The reciprocal of the slope value of the non-slice-selective inversion data in Fig. 3b, 0.413 cm^3, corresponds to an abscissa value of 4.8 cm in Fig. 4 (data point shown as a square). This means that the experiment with formally non-slice-selective inversion does in fact have an apparent selection slice 48 mm thick, in which the magnetization experiences inversion. This is in very good agreement with the 47-mm length of the RF coil used for these experiments, and with a coronal view image of the phantom sample (not shown). The S_i dependence of the data in Fig. 4 is reasonably linear when S_i is smaller than 2.0 cm, and is well approximated by the solid line calculated from the simple form of Eq. [8] that neglects the V_o term (i.e., $V^* = 0.5V_i$). However as S_i increases above 2.0 cm (in this case), the measured V^* value deviates from this theoretical value. Most generally, we can state that V^* asymptotes to $V_i/2$.

Figure 5a shows plots of R_1^* as functions of $2(S_i)^{-1}$ for different F_v values (each line is a Group I study). The R_1^* values were obtained from the data represented by filled symbols in Fig. 3b for the five S_i values not more than 2.0 cm. The symbols represent data from the experiments with F_v values of 16, 12, 10, 8.0, 6.0, 4.0 (Fig. 2c), 2.0, 1.0, and 0.0 mL/min from top to bottom, respectively. The solid lines drawn through them result from LLS fittings with the intercept held again at 0.363 s^{-1}. Only the slope, F_v/A (The *mean flow velocity*, according to the V_i term of Eqs. [1] and [8]), was varied in each fitting. The agreements are very good. Since the value of $\langle A \rangle$ calculated from these slopes is 0.12 cm^2, while the actual value for the tube is 0.11 cm^2, one can consider that the lines drawn in Fig. 5a essentially have no adjustable parameters.

Figure 5b depicts a plot of the F_v dependence of the slope (F_1) values for the R_1^* vs $2/S_i$ plots in Fig. 5a. As just stated, this slope, and hence the ordinate of Fig. 5b, can be approximated as F_v/A, the mean flow velocity. The solid line in Fig. 5b is drawn according to this approximation. Thus, its intercept is zero and its own slope is A^{-1}, as suggested above. The value of A was taken to be 0.111 cm^2 from the ID of the polyethylene tube, $\pi(3.76\ mm/2)^2$. Given that it has no adjustable parameters, the agreement of this line with the data is excellent. The systematic offset of the data from the theory is due to experimental imperfections (see below).

Finally, Figure 6 shows plots of R_1^*, obtained from the ROI containing only flowing water, as a function of S_o/S_i for $F_v = 0.1$ mL/s. The open diamonds represent data from Group I experiments in which S_o was kept at 10 mm and S_i was varied, while the filled squares and circles data from Group II studies in which S_o was varied and S_i was constant at 20 and 40 mm, respectively. The dashed lines are intended only to guide the eye. It is very clear that when $S_i \geq S_o$ the apparent relaxation rate constant depends on S_i but not noticeably on S_o. This finding is very intriguing, and strongly supports our simple model that V_i is the critical variable.

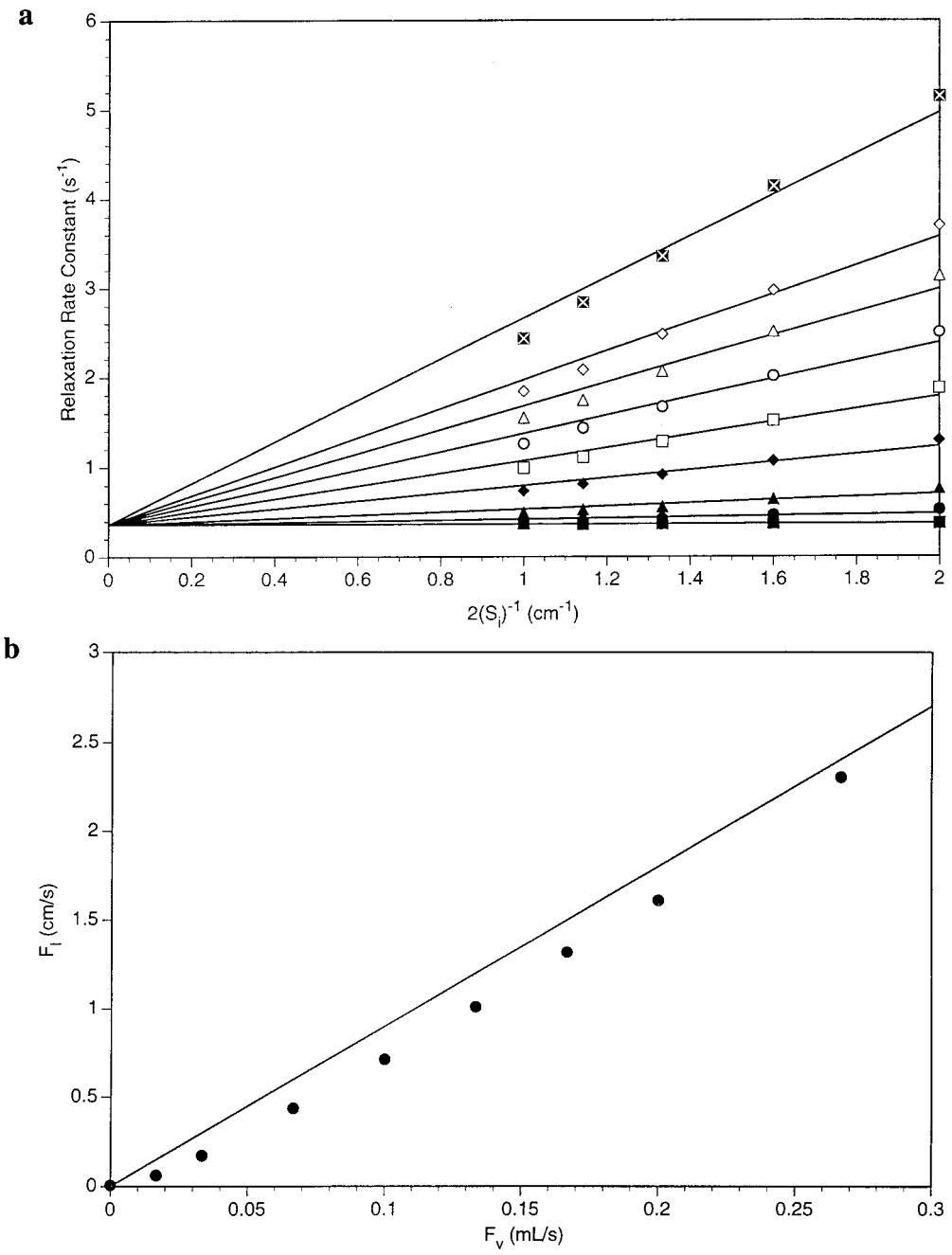

FIG. 5. (a) Plots of the $2/S_i$ dependence of the apparent R_1 values obtained from relaxograms of flowing water. The symbols represent data from the experiments with F_v of 16, 12, 10, 8.0, 6.0, 4.0 (Fig. 2c), 2.0, 1.0, and 0.0 mL/min from top to bottom, respectively. The solid lines result from LLS fittings with the intercept held at 0.363 s^{-1}. However, they are also essentially calculated with no adjustable parameters. See text. (b) Plots of the slope (F_1) values of the lines from the R^* vs $2/S_i$ plots of (a) as a function of F_v (filled circles). The solid line is calculated as F_v/A, using the cross-sectional area, $A = 0.111$ cm^2, of the tube with the flowing fluid. Since this line must go through the origin, it has no adjustable parameters.

DISCUSSION

The results in Figs. 2–5 demonstrate that flow relaxography, as accomplished by CONTIN analysis, can be very quantitatively accurate. From Fig. 3a, we learn that relaxography can quantitatively separate the NMR signals of flowing and stationary spins if the value of F_v is large enough that the ratio of T_{1L}/T_{1S} is greater than 3. For an F_v value above this threshold point, the peak area fractions become the "true" values, if comparable (Fig. 3a inset). Importantly, however, the signals

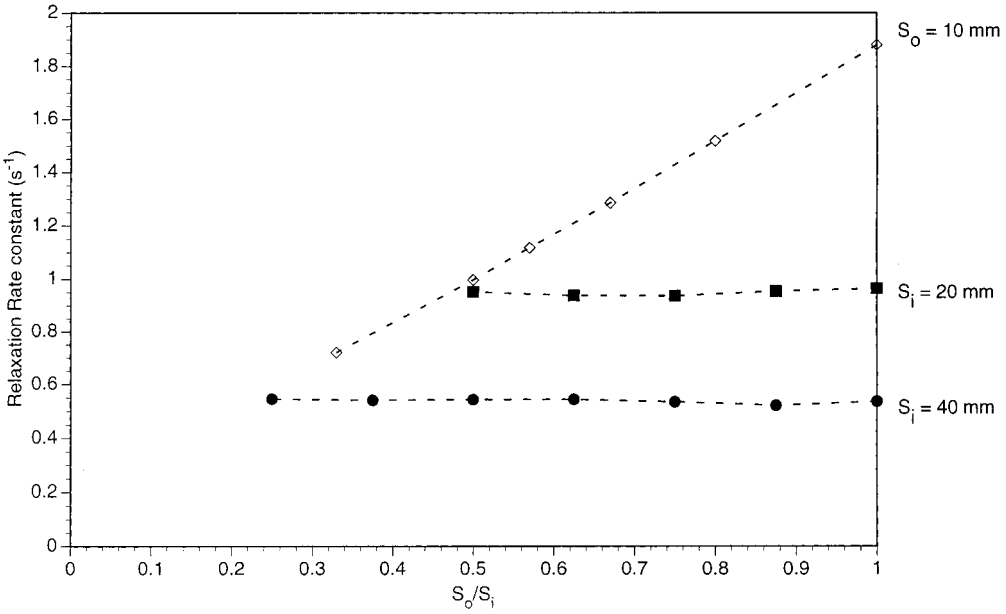

FIG. 6. Plots of the apparent relaxation rate constant of flowing water as a function of S_o/S_i. The flow rate was constant at 6.0 mL/min. The open diamonds represent data from experiments in which S_o was kept constant at 10 mm and S_i was varied (Fig. 5a), while the filled squares and circles represent data from experiments in which S_o was varied and S_i was held constant at 20 and 40 mm, respectively. The dashed lines are intended only to guide the eye.

can still be discriminated even at lower T_{1L}/T_{1S} values. The fact that the T_{1S}^{-1} values extrapolate to the independently measured "stationary" value (0.363 s^{-1}) (this is also seen in Figs. 3b and 5a) means that T_1^* values returned by CONTIN can be used to measure absolute flow rates. The agreement between theory and experiment seen in Fig. 5b reinforces this.

The fact that a good correlation between theory and experiment is observed in Figs. 3–6 also indicates that our very simple model is remarkably good at describing the longitudinal relaxation processes associated with flow-induced coherent motion in NMR. It is clear that the apparent R_1 is solidly correlated with F_v. However, the observed R_1 does not read the F_v directly: the quantities T_1 and V^* must also be known.

The value of T_1 for blood ^1H_2O is difficult to measure *in vivo*, since the experimenter may not stop the blood flow. Thus, most investigators assume it to be the same as the value measured *ex vivo*. However, Eq. [1] suggests that one can obtain the T_1 value for blood ^1H_2O, without turning off the flow, by varying S_i, therefore V^*, and therefore r_{1F}. This has been proved and demonstrated for a phantom sample in Figs. 2c and 5a.

Also, from Eq. [1], we learn that one is still not able to extract the F_v value if one knows only the value of T_1. What is really obtained by comparing R_1 and R_1^* is the mean transit time (t_F) for approximately half the volume of fluid in which the ^1H_2O magnetization was perturbed to pass through the volume V_o. This is the same as the mean residence time of the tagged molecules in V^*, and it is this that is the reciprocal of r_{1F}. Thus, we have found that the flow relaxivity is dominated by the reciprocal of the upstream tagging volume, $(V^*)^{-1}$, which can be approximated as $(V_i/2)^{-1}$. Apparently the size of the detector, the magnitude of V_o, can often be ignored. Thus, the empirical flow relaxivity is essentially the reciprocal of half of the tagging volume, $(V_i/2)^{-1}$. This is quantitatively demonstrated in Fig. 4. If V^* is equal to V_o (as implied in the literature), the data should follow the horizontal line in Fig. 4, because V_o is held constant. It definitely does not do this.

It may seem that the determination of V_o and V_i is obvious, since the slice thickness, the RF coil length, and A quantities are all well defined. However, this is not necessarily true. First, the slice thickness profile may not be perfect (*29*). Second, the $\mathbf{B}_1$ field may not be homogenous (*12, 13*). Third, the flow pattern is never perfectly defined (*19*). Fourth, the nuclei may not be fully magnetized and/or demagnetized due to flowing fluid moving in and out during the process of RF excitation and magnetization polarization (*9*). Fifth, in any biological case, the signal from flowing spins in the detected region will compete with considerable signal from nonflowing spins (*5*). The fact that some of the data in Fig. 3b deviate from the straight lines predicted by Eq. [1] may be due to one or more of the first four factors. For example, the effective V_i (and V_o) is smaller at larger F_v because of incomplete irradiation during the long (4.5 ms) sinc-shaped pulse. Consequently, R^* increases. Thus, the difference between the calculated and measured upstream inversion volume in this study (Fig. 4) suggests that this method may be the best way to test the actual calibration of the effective detected and inversion thicknesses and/or volumes associated with flow.

In the *in vivo* application, there are other considerations to anticipate. For perfusion studies, one may have an ensemble of

vessels entering the read slab with a distribution of F_v values. Also there can be a distribution of angles at which the vessels enter the slab. The theory here was derived for flow perpendicular to the slab.

For many recent perfusion studies (*30–32*), S_o/S_i is assumed to be either 1 (slice-selective inversion, the so-called *flow sensitive* condition) or 0 (non-slice-selective inversion, the so-called *flow insensitive* condition): thus, assuming $S_i = S_o$ or $S_i \gg S_o$, respectively. But one must be cautioned that S_o/S_i is never actually equal to zero when non-slice-selective inversion is employed. This is especially true for small animal studies (*33*), since the edge effect of the typically smaller RF coil can produce selection of a large, but still finite, slice. Therefore, the blood flow rate determinations for small animals may have been overestimated by studies utilizing comparison between slice- and non-slice-selective techniques.

In conclusion, the most important finding of this study is that, in the general case, the flow relaxivity, r_{1F}, is best simply approximated as $(V_i/2)^{-1}$, although the literature would lead one to think it is $(V_o)^{-1}$. Empirically, we found that r_{1F} asymptotes to $(V_i/2)^{-1}$ regardless the size of the V_o. However, the deviation of the data from this simple theory at a larger S_i and/or F_v will need further investigation. We estimate that the error of our flow measurement is within 15%.

ACKNOWLEDGMENTS

We thank Drs. Lawrence L. Latour, for the design and supervision of the gradient set construction, Ildikó Pálya, for help in using the CONTIN program and PostScript Language, and William D. Rooney, James T. Muckerman, Marshall D. Newton, and Hoby P. Hetherington, for helpful discussions, and Messrs. Christian Labadie, for a translation of Ref. (*1*), and Charles S. Landis, for help in using IDL software. We thank the U.S. Department of Energy and its office of Biological and Environmental Research (Contract DE-AC02-98CH10884) and the National Institutes of Health (Grant R01 GM32125) for support of this work.

REFERENCES

1. P. M. Denis, G. J. Béné, and R. C. Exterman, Steady-state observation of a transitory nuclear resonance phenomenon, *Arch. Sci.* **5,** 32–34 (1952).
2. J. R. Singer, Flow rates using nuclear or electron paramagnetic resonance techniques with applications to biological and chemical processes, *J. Appl. Phys.* **31,** 125–127 (1960).
3. H. C. Dorn, Flow NMR, *in* "Encyclopedia of Nuclear Magnetic Resonance" (D. M. Grant and R. K. Harris, Eds.), Vol. 3, pp. 2026–2036, Wiley, New York (1996).
4. F. W. Wehrli, A. Shimakawa, J. R. MacFall, L. Axel, and W. Perman, MR imaging of venous and arterial flow by a selective saturation-recovery spin echo (SSRSE) method, *J. Comput. Asst. Tomog.* **9,** 537–545 (1985).
5. J. R. Singer, Blood flow rates by nuclear magnetic resonance measurements, *Science* **130,** 1652–1653 (1959).
6. W. S. McCormick and W. P. Birkmeier, Optimum detectors for the NMR flow meter, *Rev. Sci. Instrum.* **40,** 346–353 (1969).
7. R. E. Halbach, J. H. Battocletti, A. Sances, R. L. Bowman, and V. Kudravcev, Cylindrical crossed-coil NMR limb blood flowmeter, *Rev. Sci. Instrum.* **50,** 428–434 (1979).
8. R. E. Halbach, J. H. Battocletti, S. X. Salles-Cunha, and A. Sances, The NMR blood flowmeter-design, *Med. Phys.* **8,** 444–451 (1981).
9. R. A. B. Devine, L. P. Clarke, S. Vaughan, and A. Serafini, Theoretical analysis of the two-coil method for measuring fluid flow using nuclear magnetic resonance, *Med. Phys.* **9,** 668–672 (1982).
10. G. Suryan, Nuclear resonance in flowing liquids, *Proc. Indian Acad. Sci. Sect. A* **33,** 107–111 (1951).
11. D. W. Arnold and L. E. Burkhart, Spin-echo NMR response from a flowing sample, *J. Appl. Phys.* **36,** 870–871 (1965).
12. M. A. Hemminga, P. A. De Jager, and A. Sonneveld, The study of flow by pulsed nuclear magnetic resonance. I. Measurement of flow rates in the presence of a stationary phase using a difference method, *J. Magn. Reson.* **27,** 359–370 (1977).
13. R. A. B. Devine, L. P. Clarke, S. Vaughan, and A. N. Serafini, Theoretical and experimental analysis of the single-coil pulsed-NMR method for measuring fluid flow, *J. Nucl. Med.* **23,** 1020–1024 (1982).
14. E. O. Stejskal, Use of spin echoes in a pulsed magnetic-field gradient to study anisotropic, restricted diffusion and flow, *J. Chem. Phys.* **43,** 3597–3608 (1965).
15. K. J. Packer, The study of slow coherent molecular motion by pulsed nuclear magnetic resonance, *Mol. Phys.* **17,** 355–368 (1969).
16. T. Grover and J. R. Singer, NMR spin-echo flow measurements, *J. Appl. Phys.* **42,** 938–940 (1971).
17. J. R. Singer, NMR diffusion and flow measurements and an introduction to spin phase graphing, *J. Phys. E. Sci. Instrum.* **11,** 281–291 (1978).
18. M. H. Buonocore, Visualizing blood flow patterns using streamlines, arrows, and particle paths, *Magn. Reson. Med.* **40,** 210–226 (1998).
19. M. A. Hemminga, Measurement of flow characteristics using nuclear magnetic resonance, *in* "Biomedical Magnetic Resonance" (T. L. James and A. R. Margulis, Eds.), pp. 157–186, Radiology Research and Education Foundation, San Francisco (1984).
20. S-G. Kim and N. V. Tsekos, Perfusion imaging by a flow-sensitive alternating inversion recovery (fair) technique: Application to functional brain imaging, *Magn. Reson. Med.* **37,** 425–435 (1997).
21. E. M. Haacke, W. Lin, and D. Li, Flow in whole body magnetic resonance, *in* "Encyclopedia of Nuclear Magnetic Resonance" (D. M. Grant and R. K. Harris, Eds.), Vol. 3, pp. 2037–2047, Wiley, New York (1996).
22. H. Y. Carr and E. M. Purcell, Effect of diffusion on free precession in nuclear magnetic resonance experiments, *Phys. Rev.* **94,** 630–635 (1954).
23. K. J. Packer, Diffusion & flow in fluids, *in* "Encyclopedia of Nuclear Magnetic Resonance" (D. M. Grant and R. K. Harris, Eds.), Vol. 3, pp. 1615–1626, Wiley, New York (1996).
24. J-H. Lee, C. Labadie, C. S. Springer, and G. S. Harbinson, Two-dimensional inverse Laplace transform NMR: Altered relaxation times allow detection of exchange correlation, *J. Am. Chem. Soc.* **115,** 7761–7764 (1993).
25. C. Labadie, J-H. Lee, G. Vétek, and C. S. Springer, Relaxographic imaging, *J. Magn. Reson. B* **105,** 99–112 (1994).
26. D. W. Jones and T. F. Child, NMR in flowing systems, *in* "Advances in Magnetic Resonance" (J. S. Waugh, Ed.), Vol. 8, pp. 123–148, Academic Press, New York (1976).
27. A. N. Garroway, P. K. Grannell, and P. Mansfield, Image formation

in NMR by a selective irradiative process, *J. Phys. C* **7,** L457–L462 (1974).

28. K. P. Whittall and A. L. Mackay, Quantitative interpretation of NMR relaxation data, *J. Magn. Reson.* **84,** 134–152 (1989).
29. R. R. Edelman, H. P. Mattle, J. Kleefield, and M. S. Silver, Quantification of blood flow with dynamic MR imaging and presaturation bolus tracking, *Radiology* **171,** 551–556 (1989).
30. J. A. Detre, J. S. Leigh, D. S. Williams, and A. P. Koretsky, Perfusion imaging, *Magn. Reson. Med.* **23,** 37–45 (1992).
31. S-G. Kim, Quantification of relative blood flow change by flow-sensitive alternating inversion recovery (fair) technique: Application to functional mapping, *Magn. Reson. Med.* **34,** 293–301 (1995).
32. K. K. Kwong, D. A. Chesler, R. M. Weisskoff, K. M. Donahue, T. L. Davis, L. Ostergaard, T. A. Campbell, and B. R. Rosen, MR perfusion studies with T_1-weighted echo planar imaging, *Magn. Reson. Med.* **34,** 878–887 (1995).
33. C. Schwarzbauer, S. P. Morrissey, and A. Haase, Quantitative magnetic resonance imaging of perfusion using magnetic labeling of water proton spins within the detection slice, *Magn. Reson. Med.* **35,** 540–546 (1996).